Suitability of the new generation of SAR satellites to the wetland InSAR application

Shimon Wdowinski[1], San-Hoon Hong[2], Brian Brisco[3]

1. **University of Miami**
2. **Korea Aerospace Research Institute**
3. **Canada Centre for Remote Sensing**

- Wetland InSAR
- The new generation of SAR satellites
- New observations
- Summary & acknowledgements

Wetland InSAR

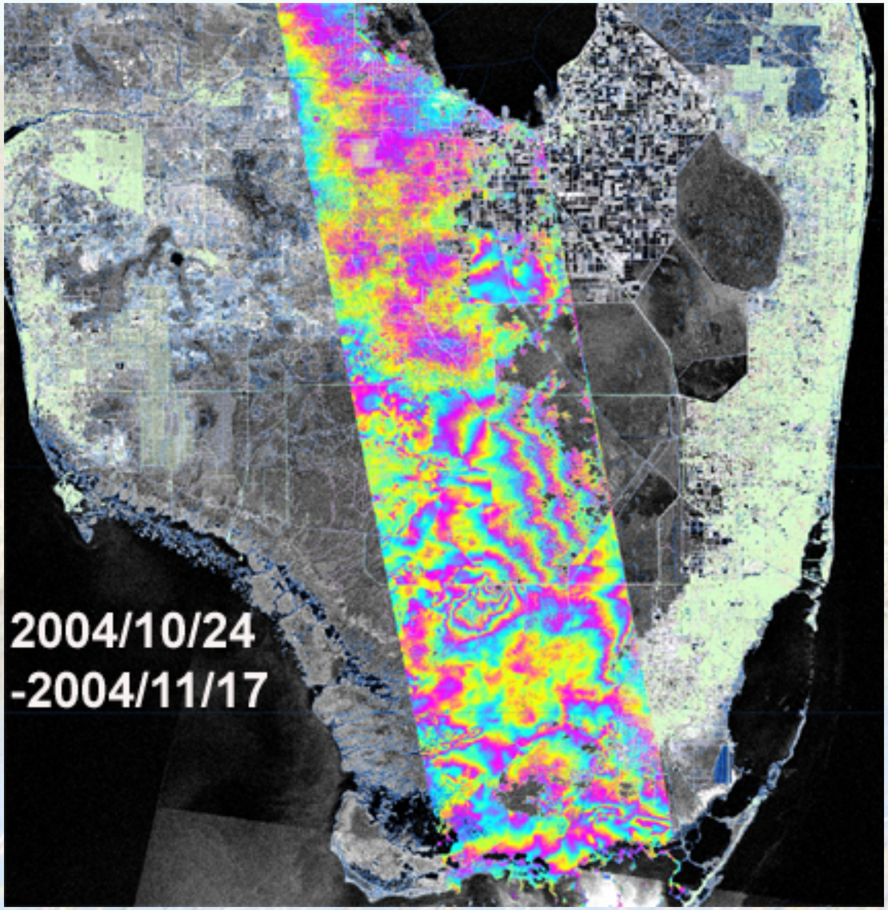

Double bounce effect

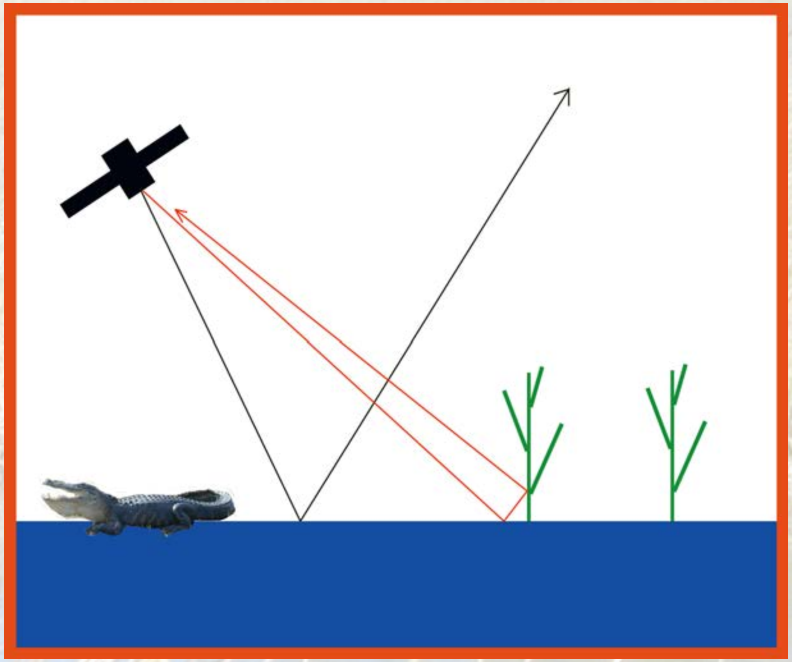

Using InSAR observations to detect surface water level changes in wetlands

Water level change measurements♪

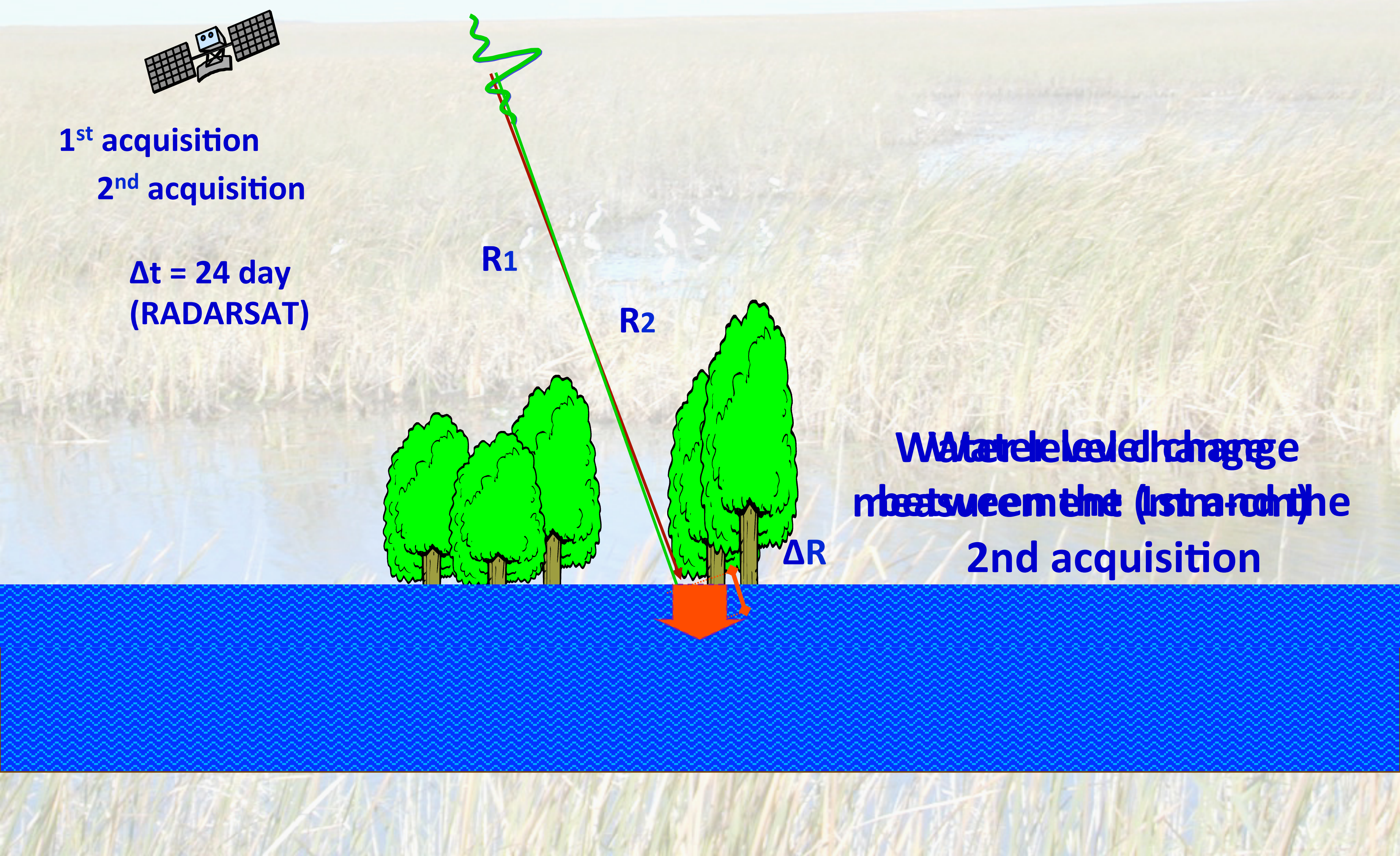

South Florida wetlands as a natural laboratory

South Florida

- Various environments:
  - •Wetlands
  - •Agriculture
  - •Urban
- Various wetland types
  - •Woody
  - •Herbaceous
  - •Mangrove
- Various wetland environments
  - •Natural
  - •Controlled
- Dense stage station network

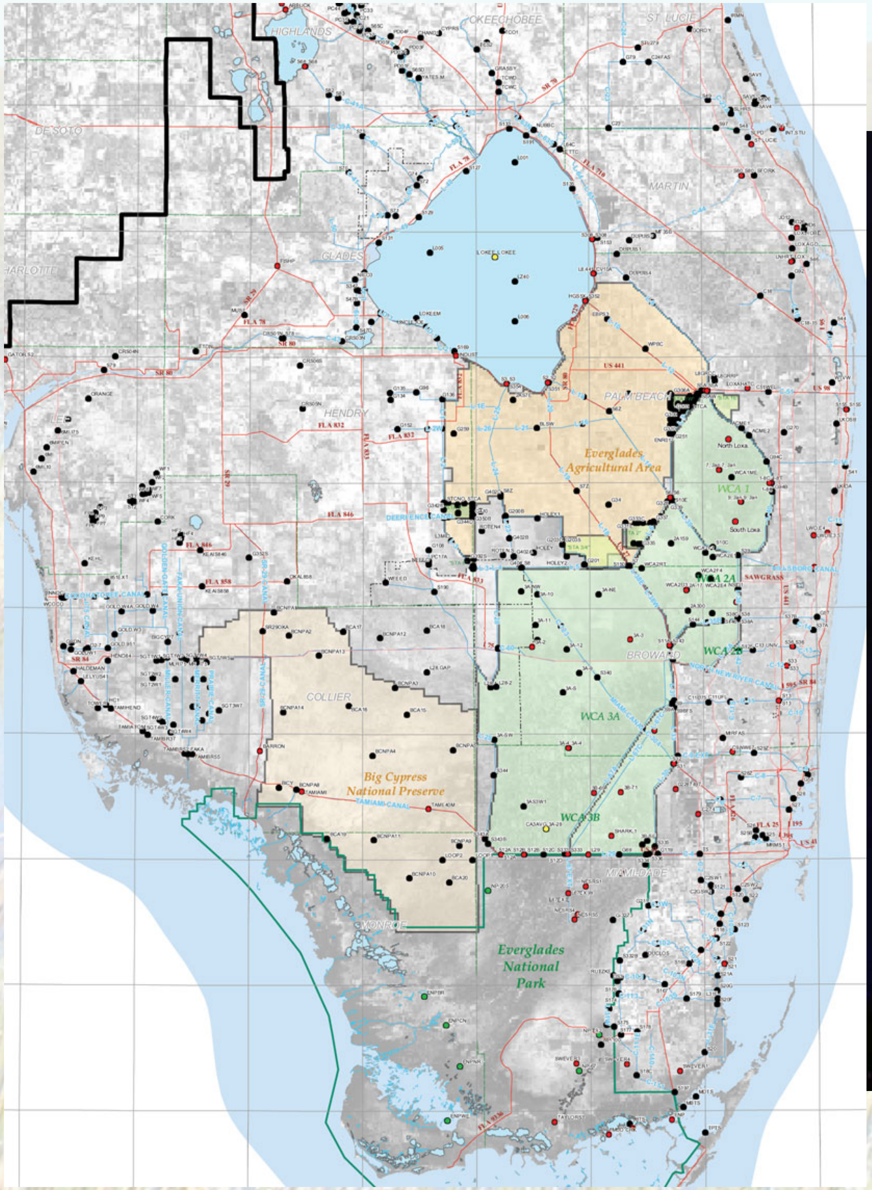

Water level changes

Interferogram

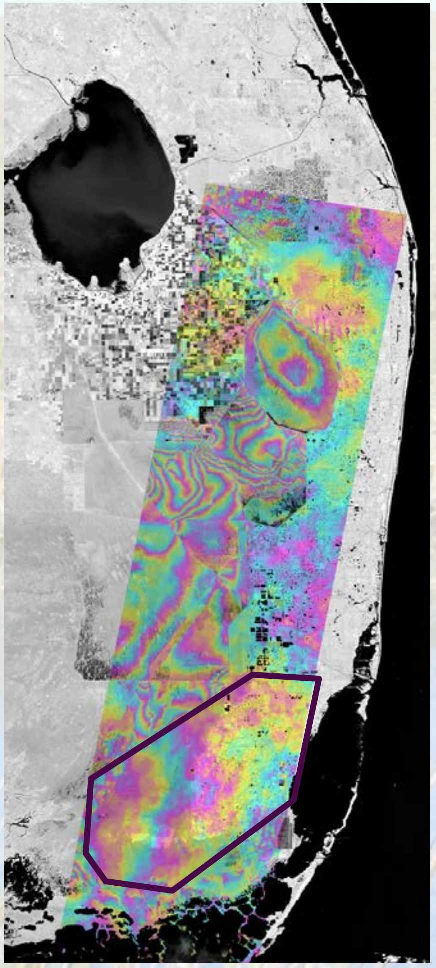

Calibration with stage data

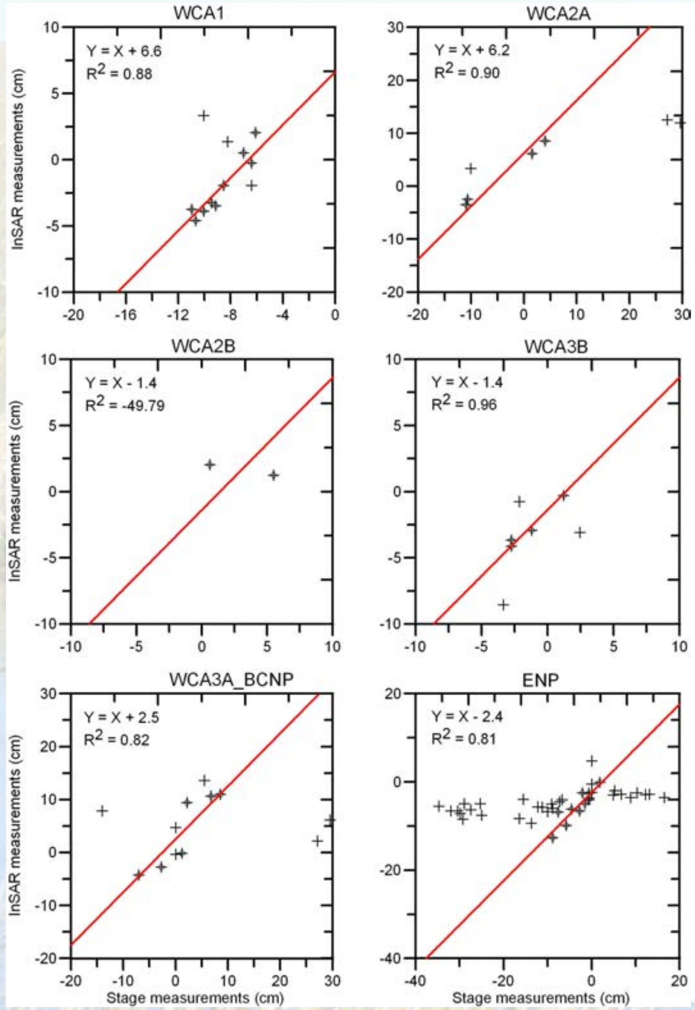

Change maps

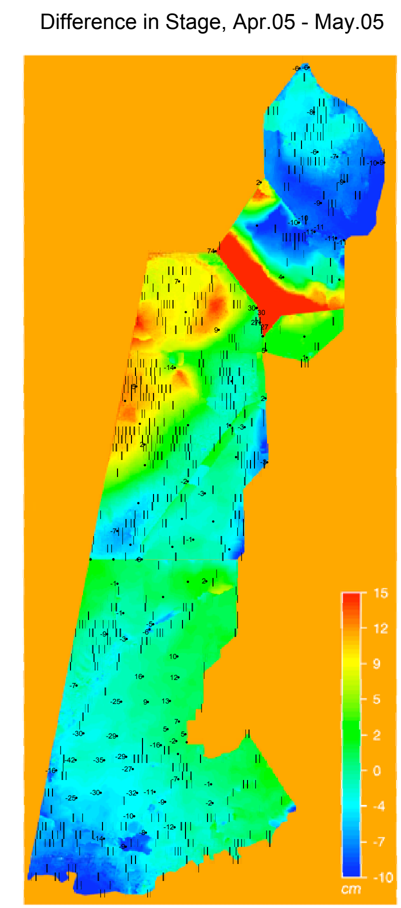

InSAR time series (STBAS)

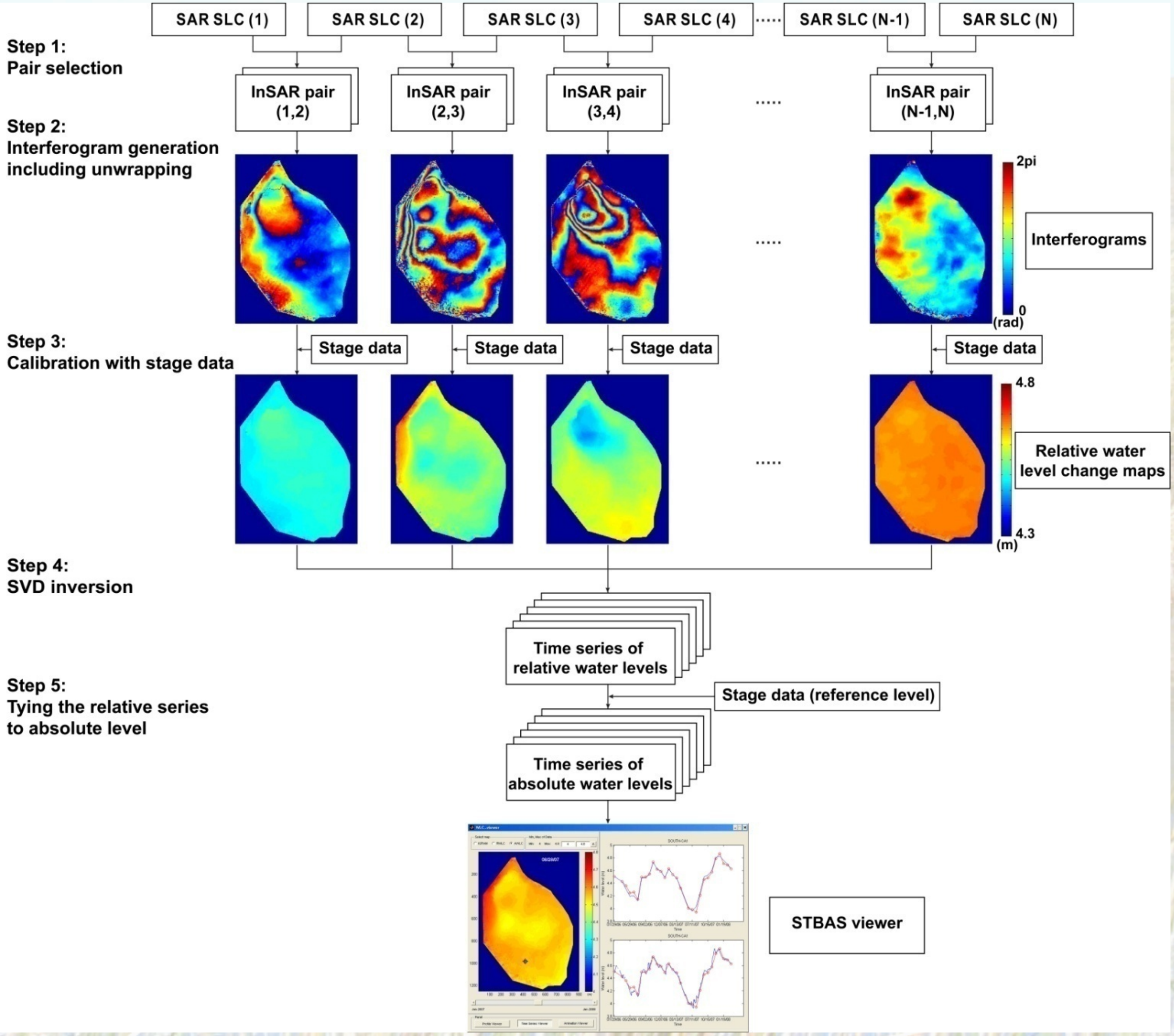

Hong et al. (2010)

Time series of water levels♪

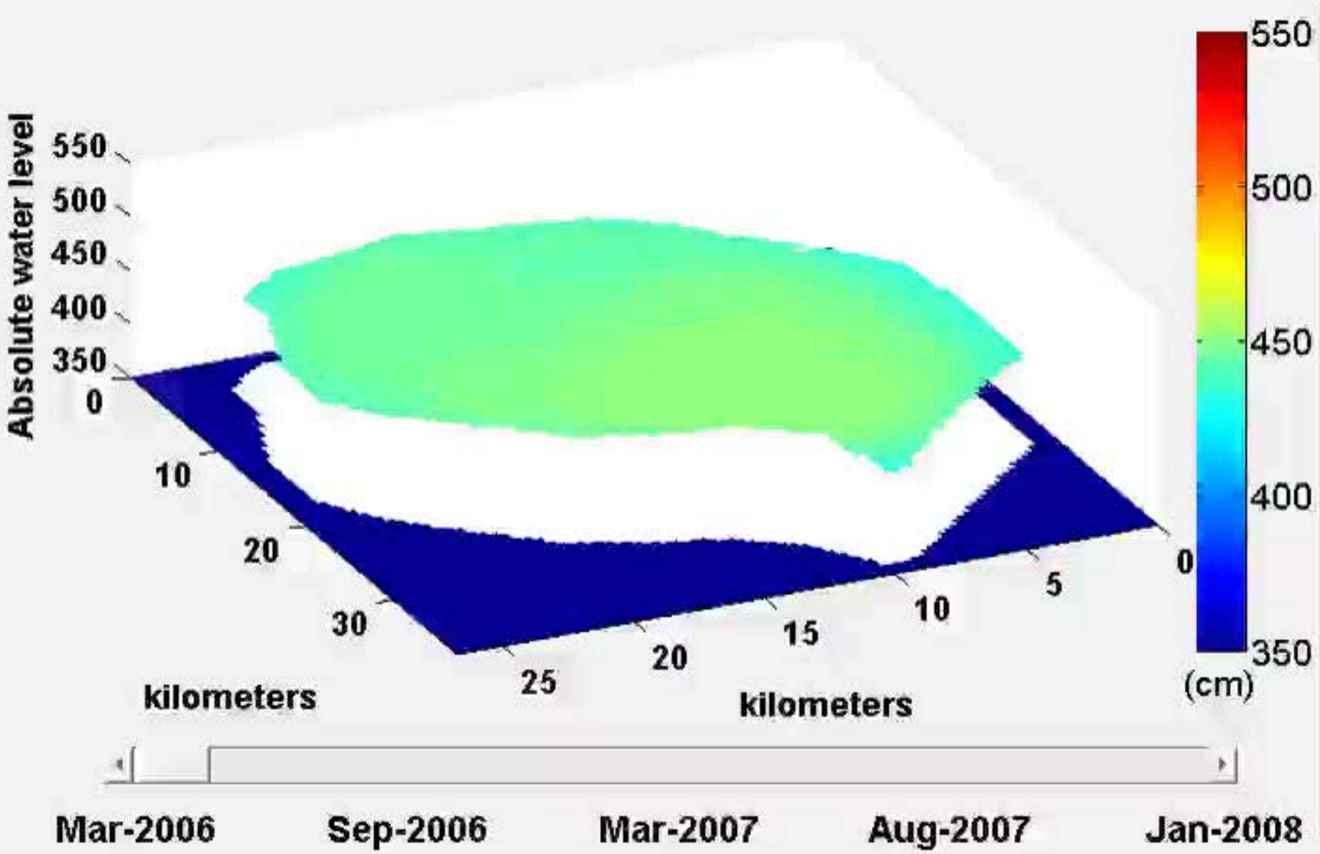

SAR satellites

First generation:

(SEASAT)
ERS-1/2
JERS-1
RADARSAT-1
ENVISAT

C-, L-band
Single/dual polarization
10-50 m resolution
24, 35, 46 day repeat path

Second generation:

ALOS/PALSAR
TSX/TDX
CosmoSky-Med
RADARSAT-2

X-, C-, L-band
Dual/Quad polarization
1-50 m resolution
1-46 day repeat path

Planned missions:

Sentinel-1
ALOS-2
TerraSAR-X2
CRM
DESDeNI

X-, C-, L-band
Dual/Quad/Compact pol.
1-50 m resolution
Constellations

SAR sensor and vegetation

Short wavelength radar signal interacts more with vegetation and tends to back-scatter from tree canopies

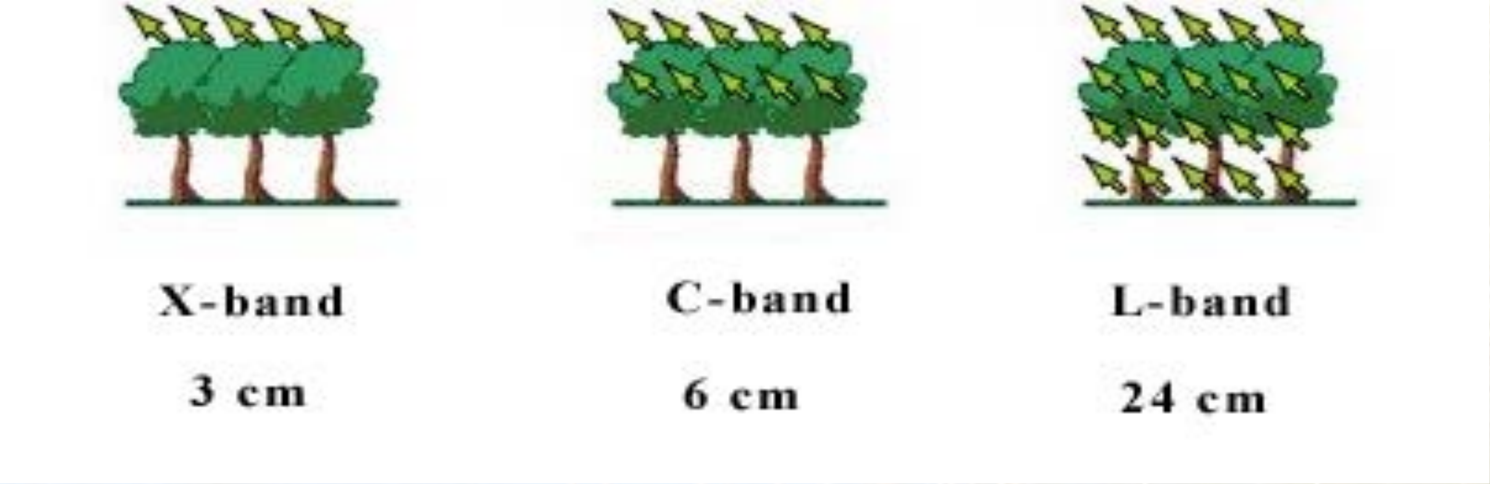

- L-band data is most suitable for wetland InSAR.
- C-band also works fairly well, especially with HH polarization and short temporal baseline.
- X-band – Surprisingly also works very well.

L-, C-, and X-band Interferograms

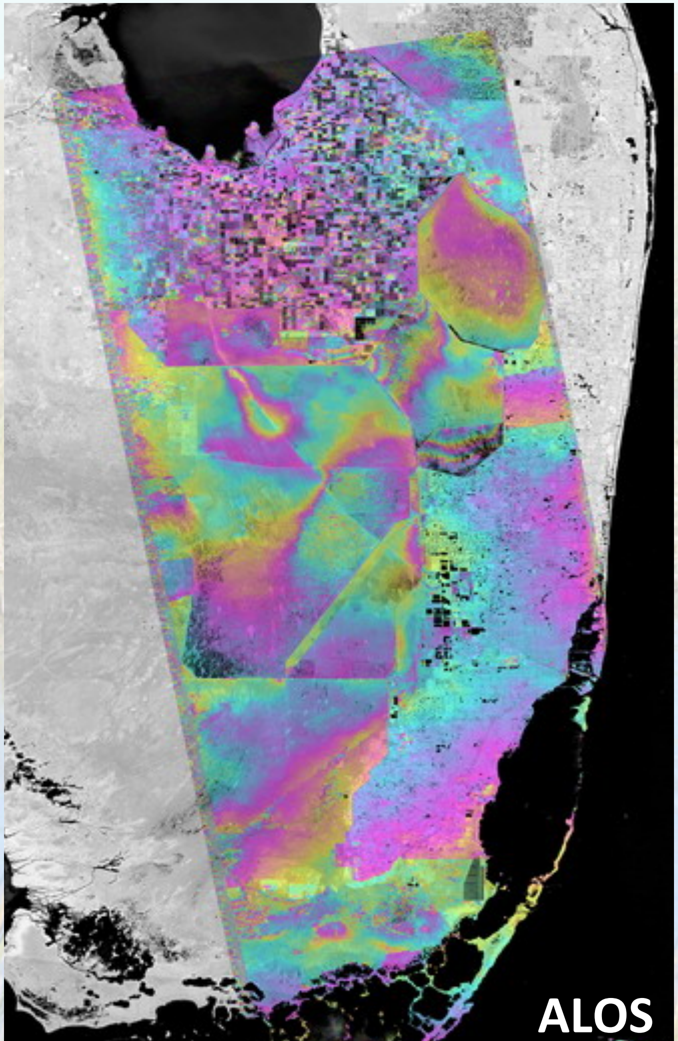

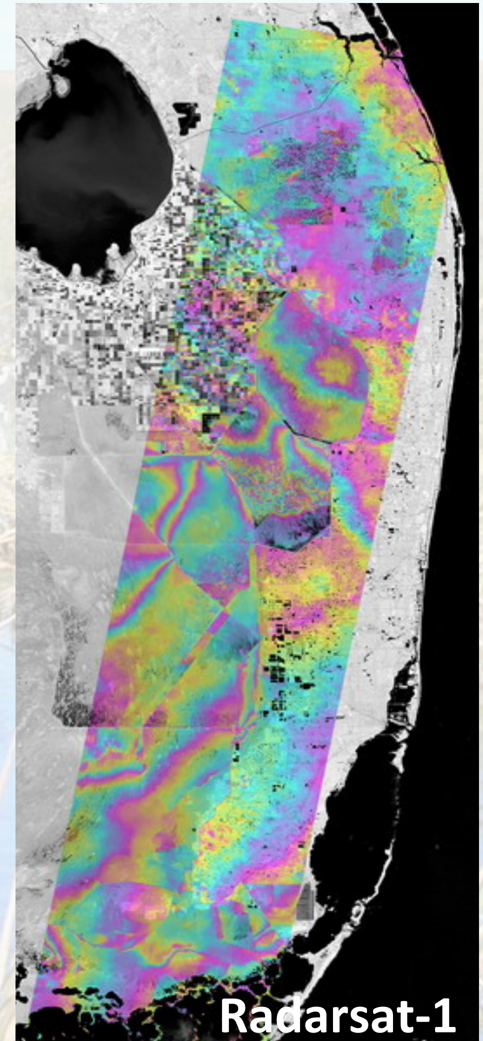

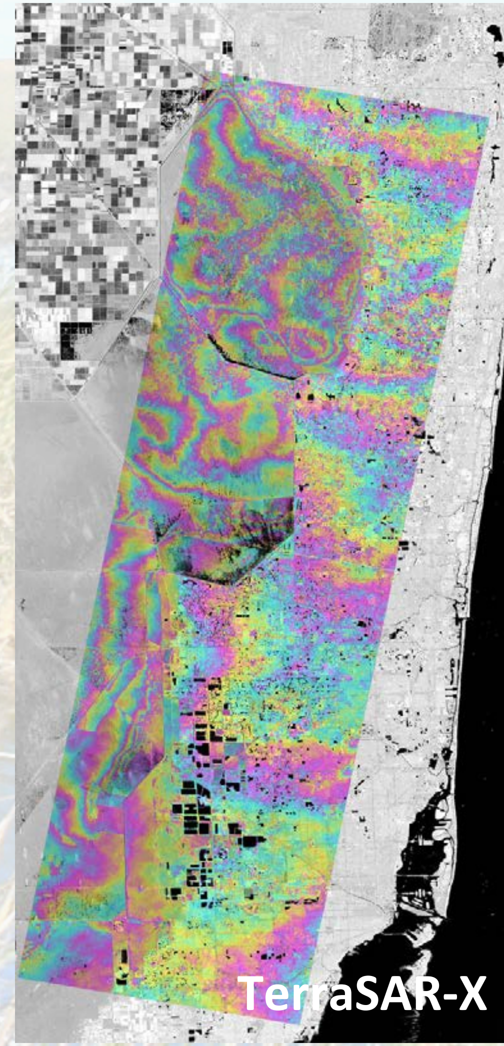

High spatial resolution maps of water level changes.
Vertical change (fringes): L-band – 15 cm; C-band – 4 cm; X-band – 2 cm

TerraSAR-X Dual polarimetric data

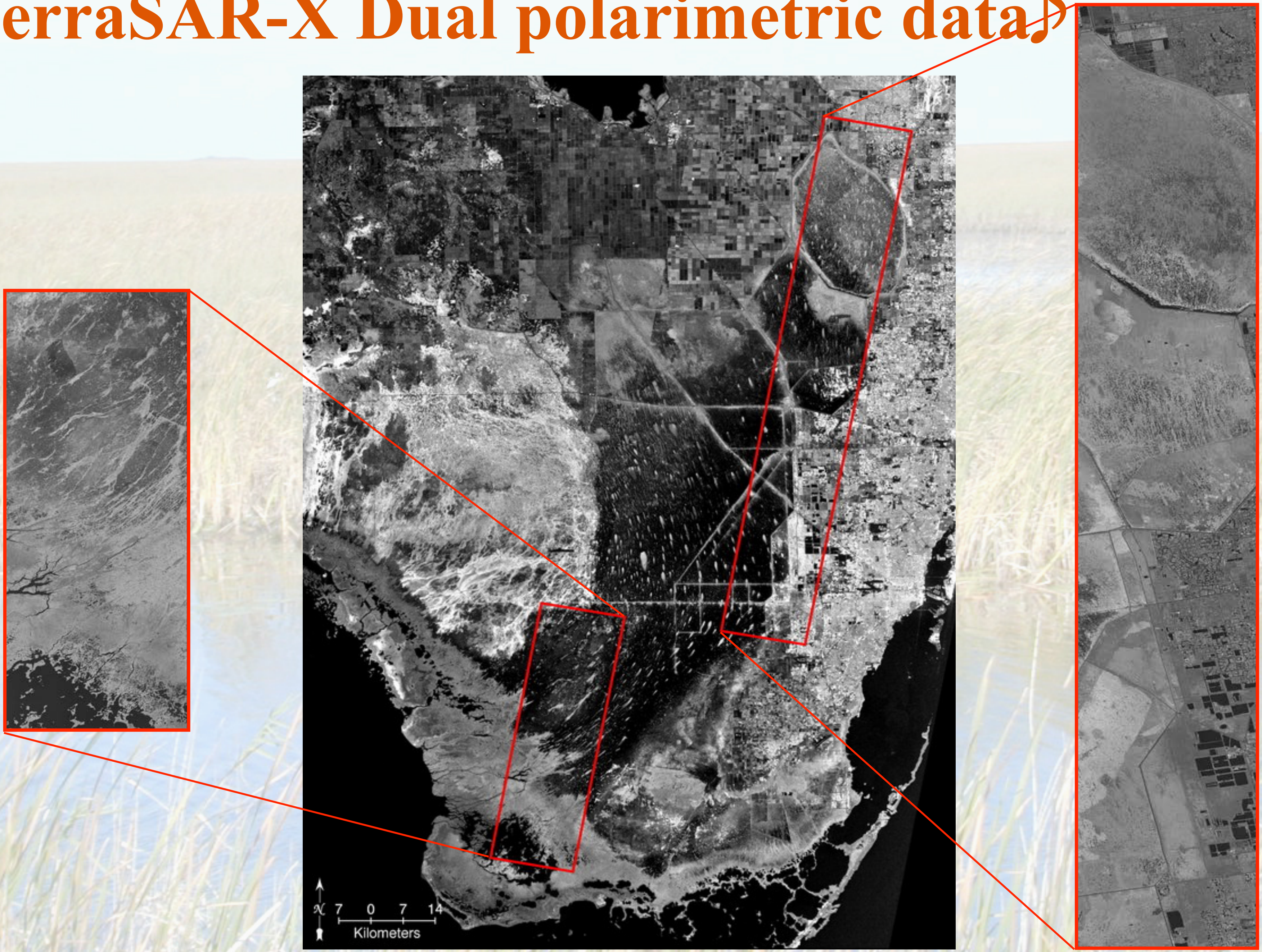

Water Conservation Area (WCA) Managed wetland♪

- Water level changes can be detected at all polarimetric data.

- The coherence are the best in HH-pol, and VV is the next. The cross-pol has the lowest coherence.

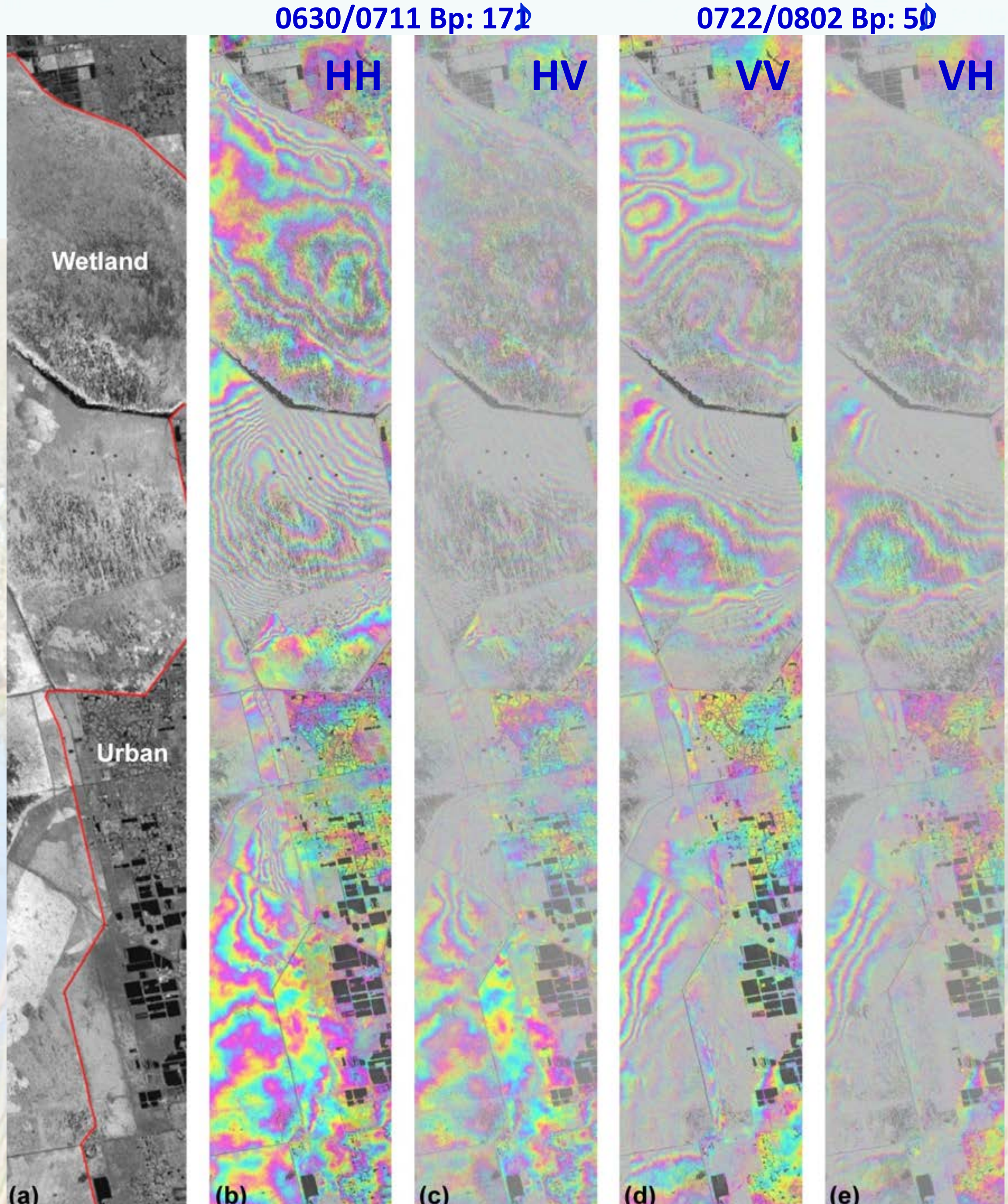

Freshwater wetland v.s. Saltwater mangrove♪

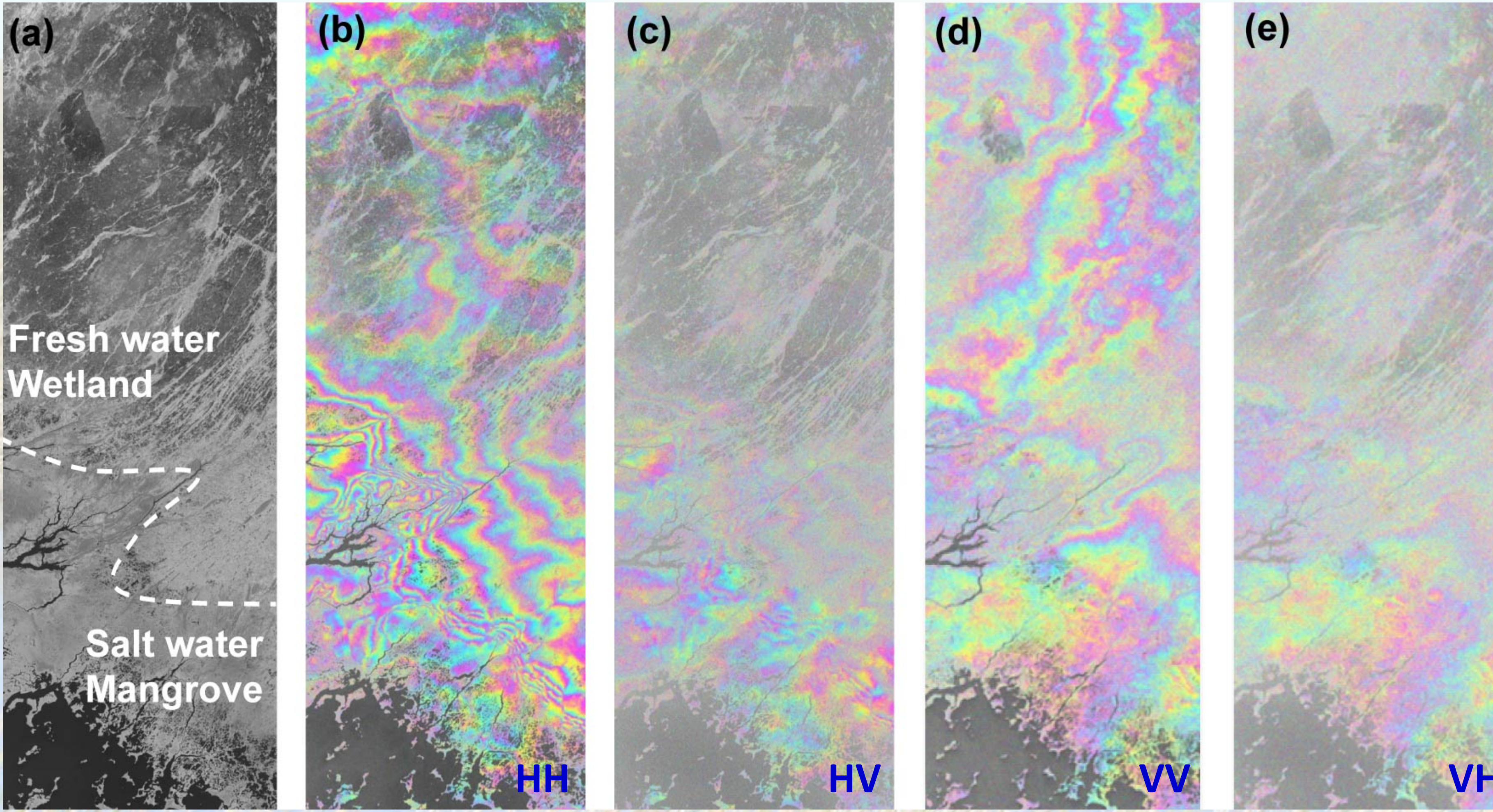

0926/1007 Bp: 7♪

1109/1120 Bp: 14♪

- Cross-pol acts like double bounce scattering as well as volume scattering

Radarsat-2 Quad-pol, Fine beam mode (5 m)♪

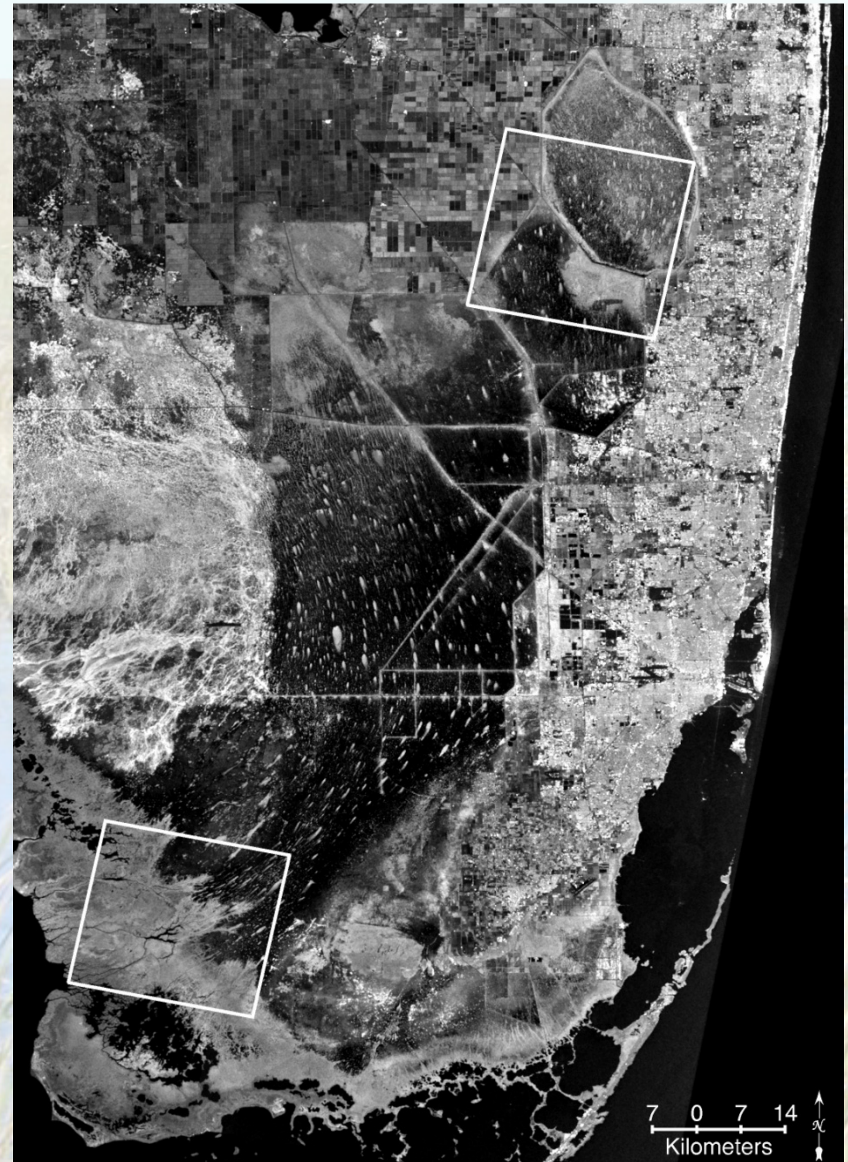

Managed wetland

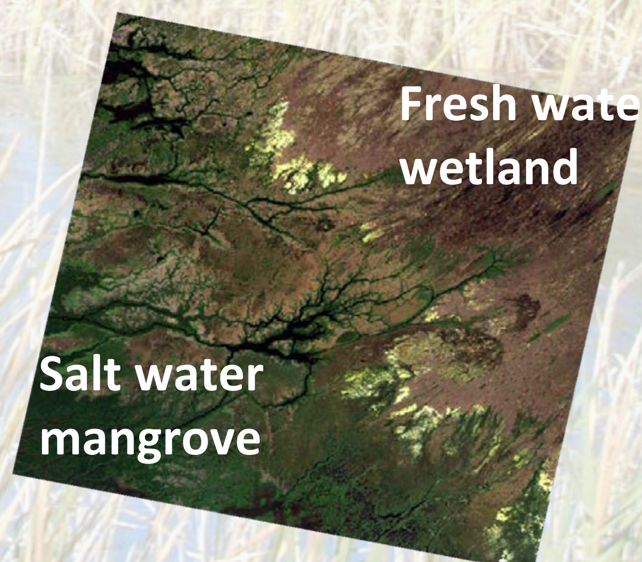

Slough + Mangrove

Radarsat-2: Fine Quad-pol mode (5 m)♪

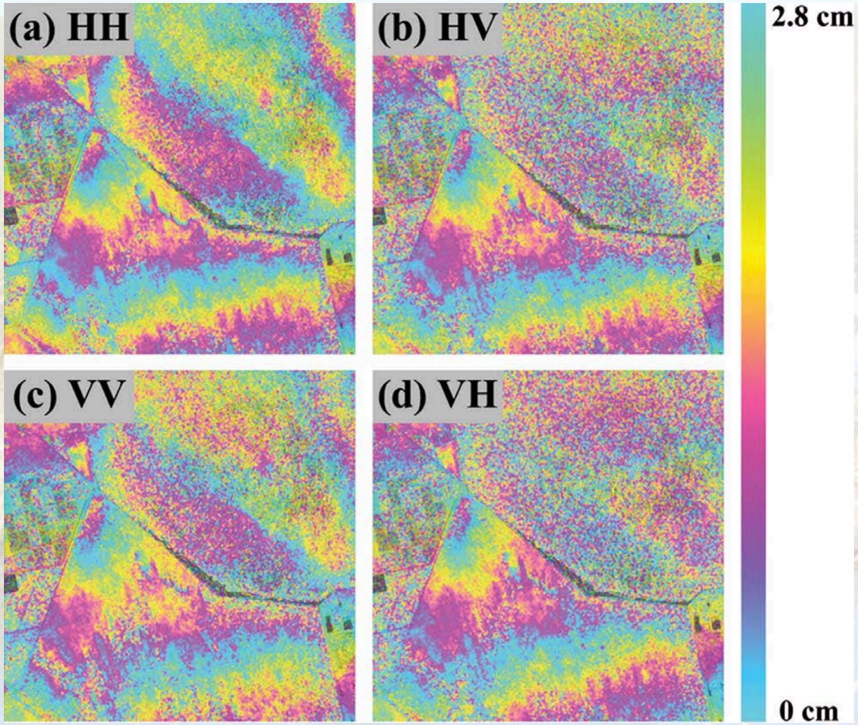

Managed wetlands

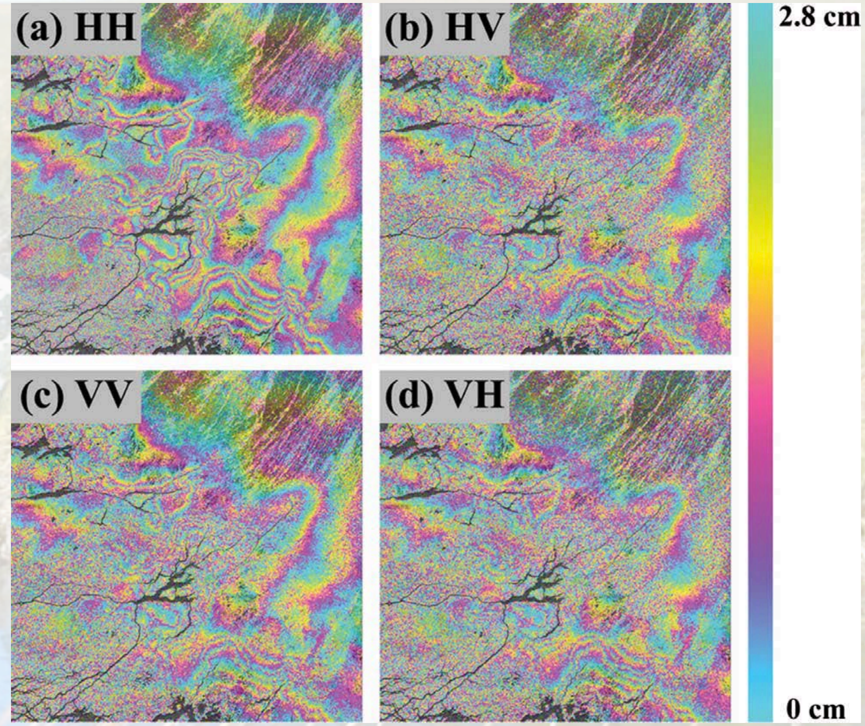

Rural wetlands

Surprising result: Cross-pol interferograms (volume scattering ?) show fringes due to water level changes (double bounce)

SAR vegetation scattering theory

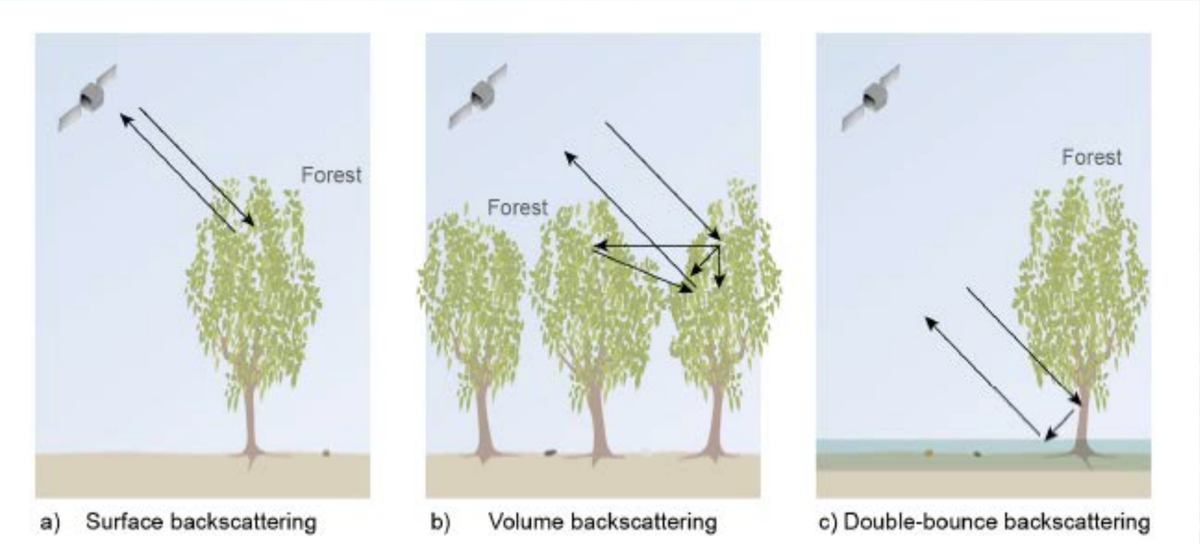

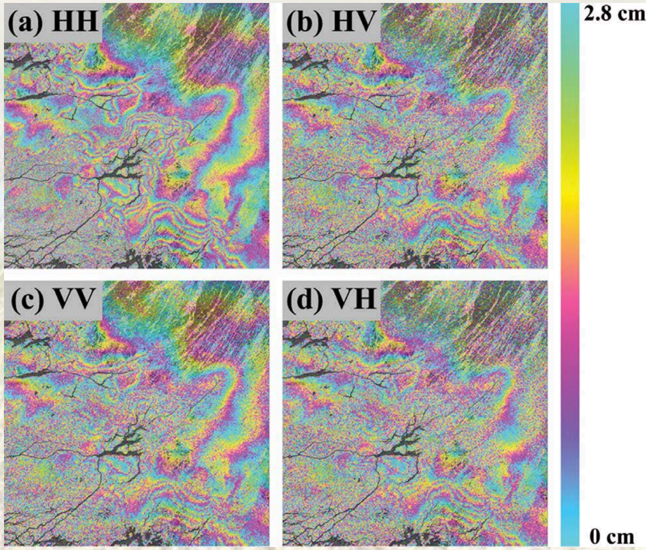

Gondwe (2010)

<u>Current assumption:</u>
Double bounce = HH-VV
Single bounce = HH+VV
Volume scattering = HV

<u>Observations:</u>
Cross-polarization (HV) interferograms show water level changes
=> *HV has a double bounce component*

Revising vegetation scattering theory♪

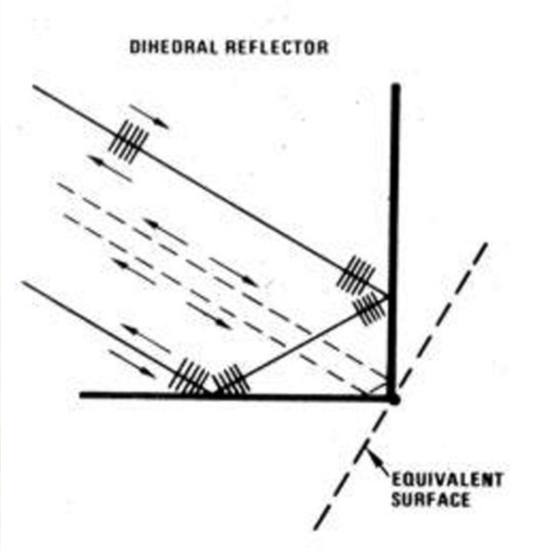

Dihedral

Hong and Wdowinski (2012)

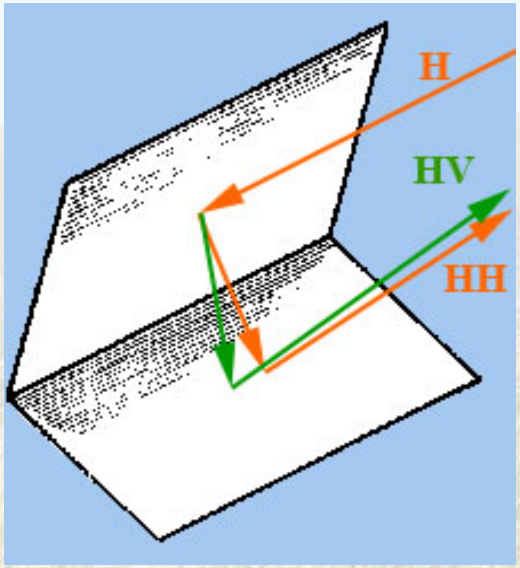

Rotated Dihedral

Cypress

Mangroves

Four component POLSAR decomposition♪

Pauli matrix:

$$\underline{k} = \frac{1}{\sqrt{2}}\begin{bmatrix} S_{HH} + S_{VV} \\ S_{HH} - S_{VV} \\ 2S_{HV} \end{bmatrix} \longrightarrow \langle |T| \rangle = \frac{1}{N}\sum_{i=1}^{N} \underline{k}\cdot\underline{k}^{*T}$$

$$\langle |T| \rangle^{HV} = \begin{bmatrix} T_{11} & T_{12} & T_{13} \\ T_{21} & T_{22} & T_{23} \\ T_{31} & T_{32} & T_{33} \end{bmatrix} = \begin{bmatrix} \frac{1}{2}\langle |S_{HH}+S_{VV}|^2 \rangle & \frac{1}{2}\langle (S_{HH}+S_{VV})(S_{HH}-S_{VV})^* \rangle & \langle (S_{HH}+S_{VV})S_{HV}^* \rangle \\ \frac{1}{2}\langle (S_{HH}-S_{VV})(S_{HH}+S_{VV})^* \rangle & \frac{1}{2}\langle |S_{HH}-S_{VV}|^2 \rangle & \langle (S_{HH}-S_{VV})S_{HV}^* \rangle \\ \langle S_{HV}(S_{HH}+S_{VV})^* \rangle & \langle S_{HV}(S_{HH}-S_{VV})^* \rangle & \langle 2|S_{HV}|^2 \rangle \end{bmatrix} = P_s[T]_{plate} + P_d[T]_{diplane} + P_v[T]_{volume}$$

$$[T]_{plate} = \begin{bmatrix} 1 & 0 & 0 \\ 0 & 0 & 0 \\ 0 & 0 & 0 \end{bmatrix} \qquad [T]_{diplane} = \begin{bmatrix} 0 & 0 & 0 \\ 0 & \cos^2 2\varphi & -\frac{\sin 4\varphi}{2} \\ 0 & -\frac{\sin 4\varphi}{2} & \boxed{\sin^2 2\varphi} \end{bmatrix} \qquad [T]_{volume} = \frac{1}{4}\begin{bmatrix} 2 & 0 & 0 \\ 0 & 1 & 0 \\ 0 & 0 & 1 \end{bmatrix}$$

Rotated dihedral from cross-pol

$$T_{11} = \frac{1}{2}\langle |S_{HH}+S_{VV}|^2 \rangle = P_s + \frac{1}{2}P_v \qquad T_{33} = 2\langle |S_{HV}|^2 \rangle = P_d \sin^2 2\varphi + \frac{1}{4}P_v$$

$$T_{22} = \frac{1}{2}\langle |S_{HH}-S_{VV}|^2 \rangle = P_d \cos^2 2\varphi + \frac{1}{4}P_v \qquad T_{23} = \mathrm{Re}\langle (S_{HH}-S_{VV})S_{HV}^* \rangle = -\frac{\sin 4\varphi}{2}$$

Ps - surface, Pd - double bounce, Pv - volume

Double bounce component can be derived from cross-pol

Testing of the decomposition♪

- SanFransisco with Radarsat-2

Ps from T_{11}

Pd from T_{22}

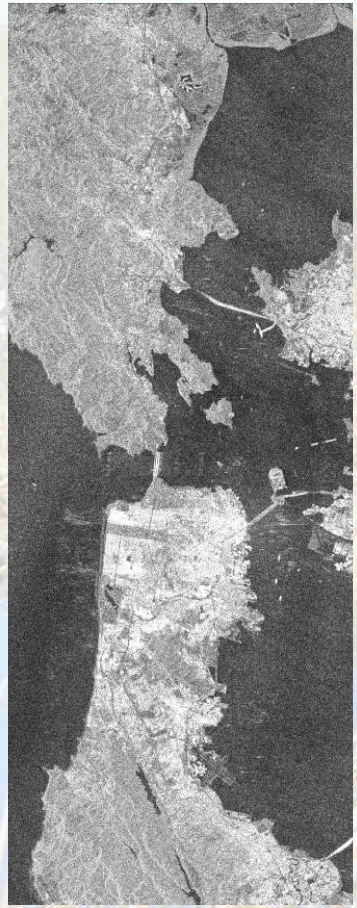

Pd from T_{33}

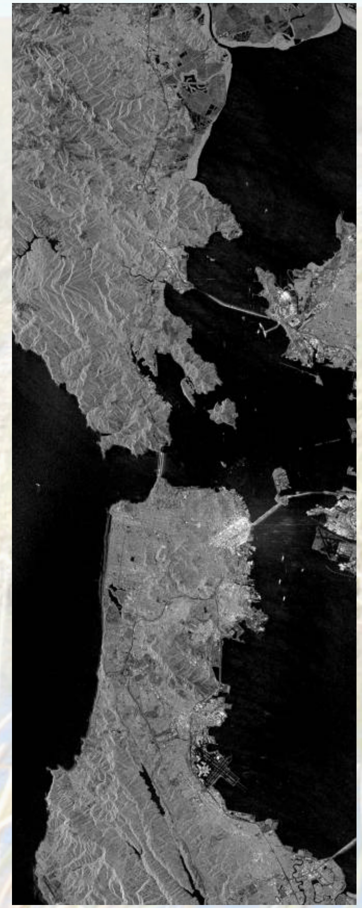

Pv from T_{33}

Color composite image
red (Pd from T_{22})
green (Pv from T_{33})
blue (Ps from T_{11})

Poster THP.P.437

Radarsat-2 HH, Wide Ultra Fine mode (8 m)♪

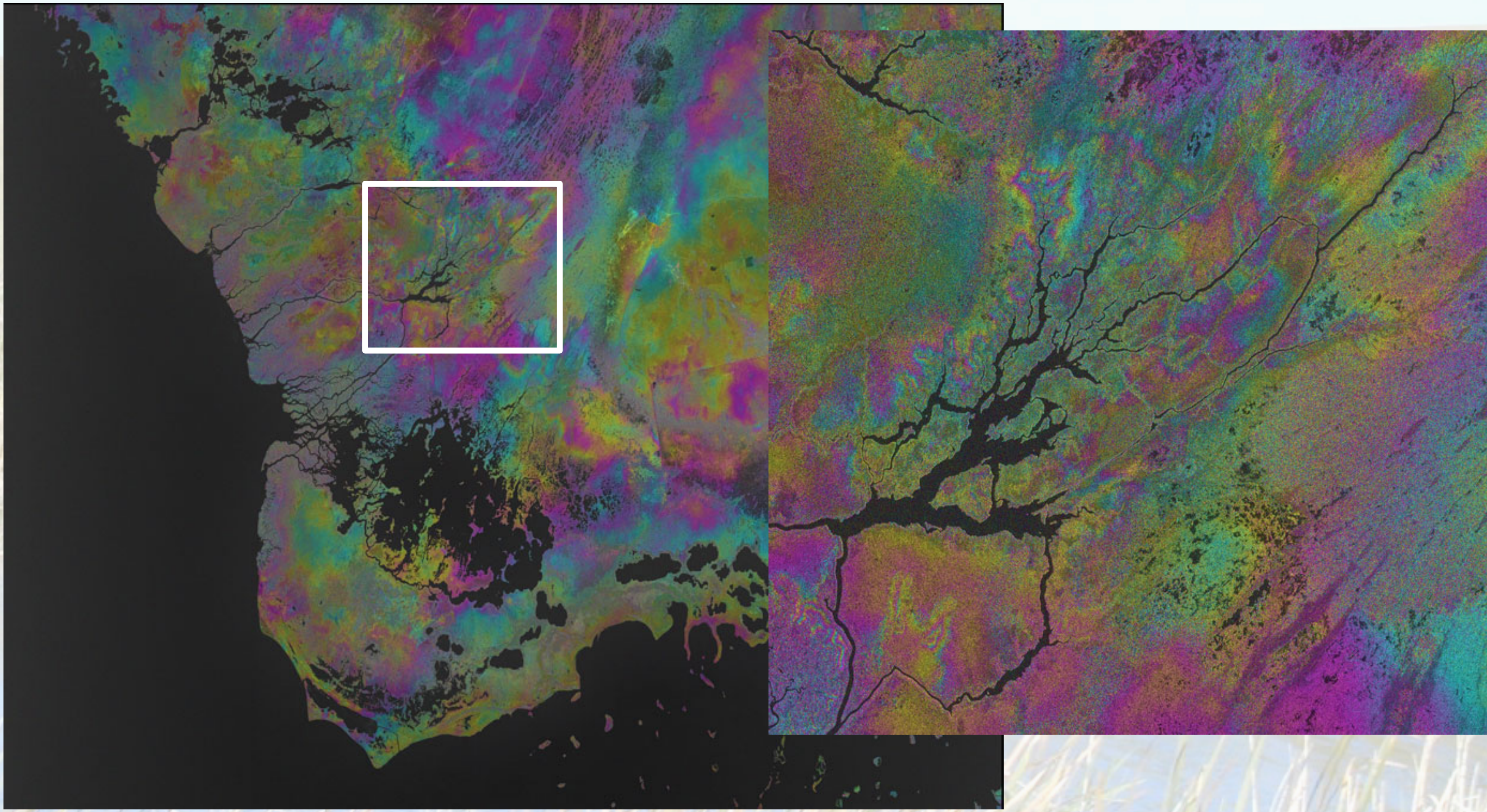

Advantage: 90 km wide swath

Radarsat-2: Wide Ultra-fine vs. Fine modes♪

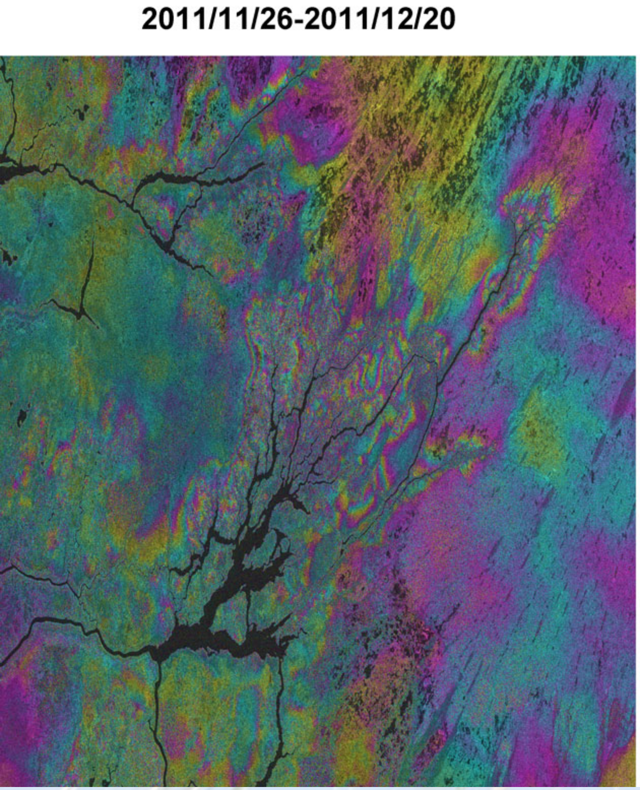

Wide Ultra-fine

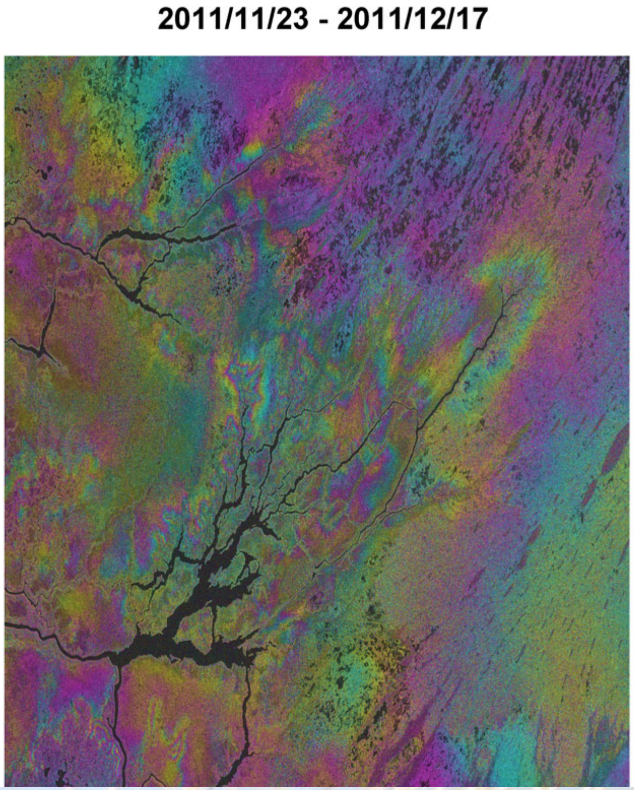

Wide Ultra-fine

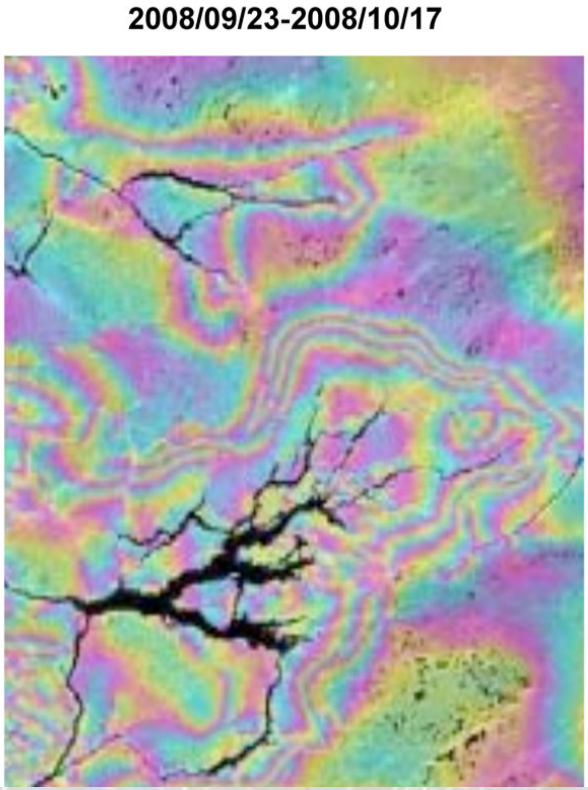

Quad-fine

Cosmo-SkyMed

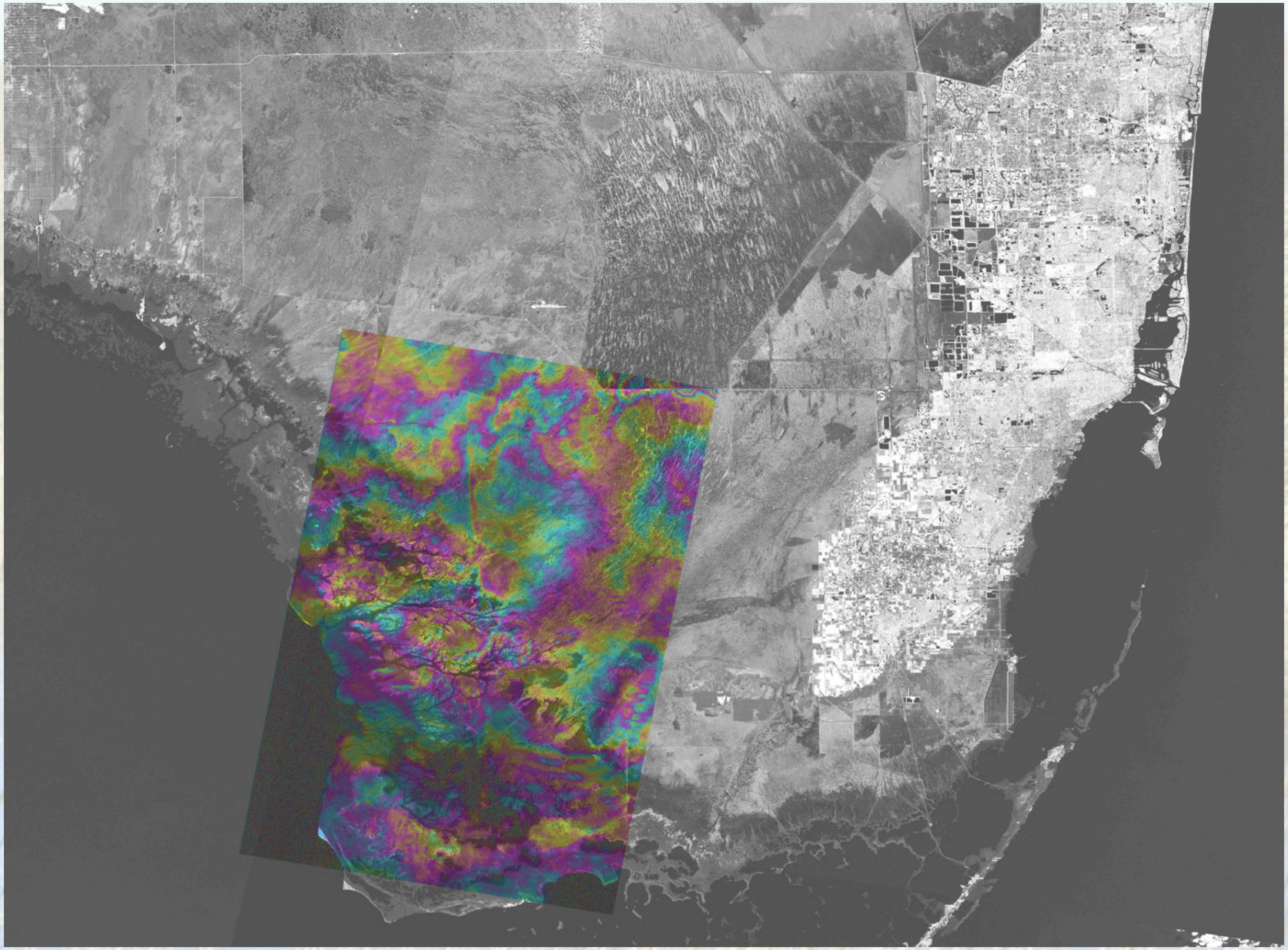

1-day interferogram (2010/11/09 – 2010/11/10)

Cosmo-SkyMed

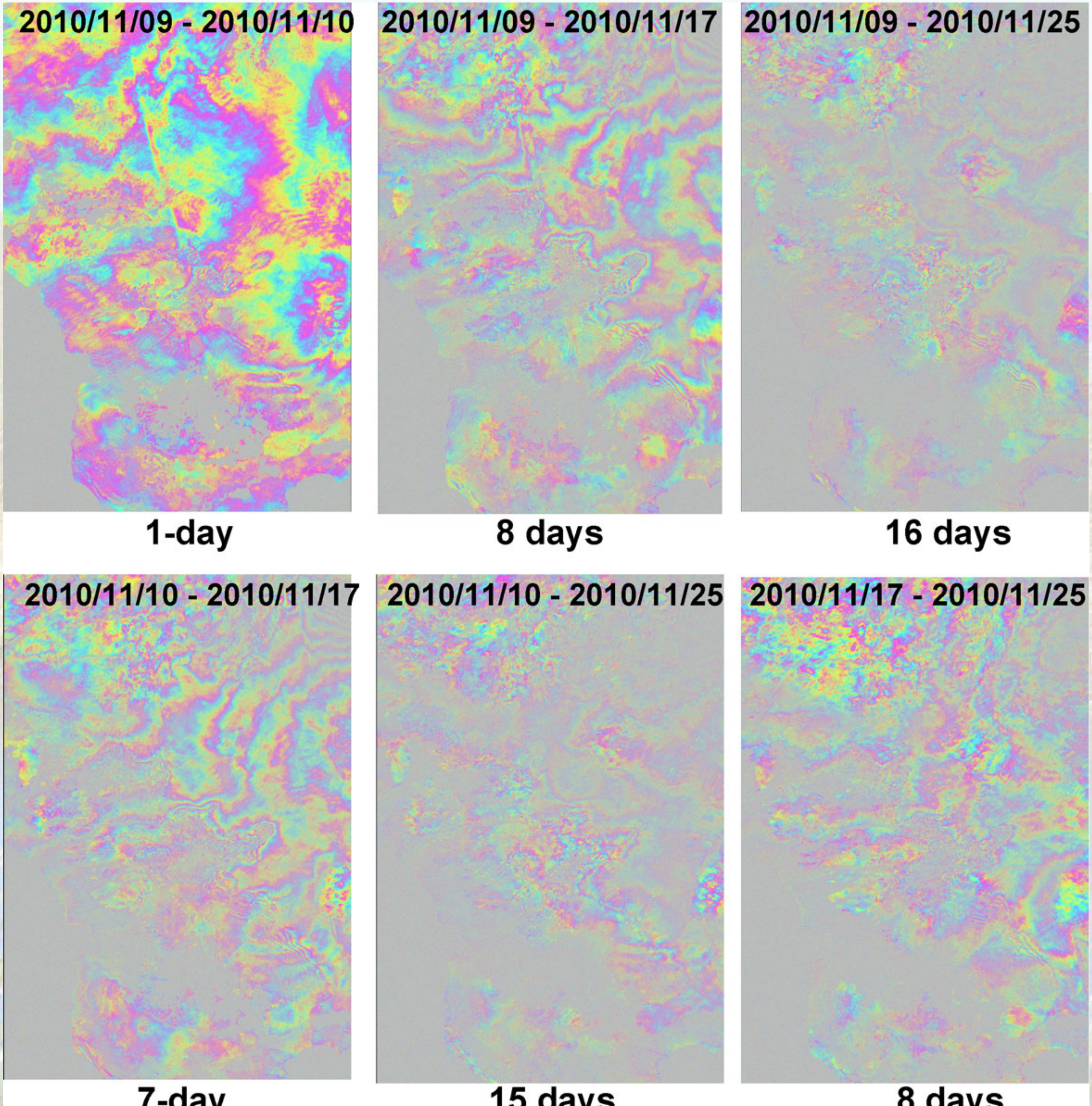

Fast coherence decay with time

No dual-pol phase observations

Summary

- **The new generation of SAR satellites can acquire data with significantly improved spatial (1-5 m) and temporal (1, 7, 8, 11… days) resolutions.**
- **The high temporal resolution observations provide high coherence with all sensor types, even X-band.**
- **The high spatial resolution observations provide very detailed information on water level changes and wetland surface flow through vegetation.**
- **The new dual- and quad-pol observations indicate that cross-pol radar signal samples the water surface beneath the vegetation, which led to the revision of vegetation scattering theory.**

Acknowledgements

SAR data

- JAXA – ALOS, L-band data
- CSA – RADARSAT-2, C-band data
- DLR – TerraSAR-X, X-band data
- ASI– Cosmo-SkyMed, X-band data

Support

- National Institute for Water Research (USGS)
- NASA
- ONR
- SFWMD